Geophys. J. Int. (2002) **149,** 454–462

A model of the geomagnetic field and its secular variation for epoch 2000 estimated from Ørsted data

Nils Olsen

Danish Space Research Institute, Juliane Maries Vej 30, DK-2100 *Copenhagen Ø, Denmark*

Accepted 2001 November 22. Received 2001 November 8; in original form 2001 July 12

SUMMARY

The availability of high-precision geomagnetic measurements from satellites such as Ørsted and CHAMP opens a new era in geomagnetic field research. However, in order to take full advantage of the improved data accuracy it is necessary to refine the usual way of deriving field models from satellite data.

This paper describes the derivation of a spherical harmonic model of the main field (up to degree/order 29) and of the secular variation (up to degree/order 13) using Ørsted data spanning more than 2 yr (1999 March–2001 September) and applying new modelling approaches for a correct statistical treatment of the data errors and for considering external field contributions. Magnetospheric contributions are modelled up to degree/order two; the zonal terms vary with annual and semi-annual periodicity, and terms with degree $n = 1$ are modulated with the strength of the magnetospheric ring current as measured simultaneously by globally distributed geomagnetic observatories. In addition, the observatory data are used to constrain secular variation.

The model is estimated using an iteratively reweighted least-squares method with *Huber weights* to account for the non-Gaussian data error distribution. The rms misfit achieved at non-polar latitudes is 3 nT for the scalar intensity and for one of the vector components perpendicular to the magnetic field; the third vector component (rms misfit of 6.4 nT owing to attitude noise) is downweighted when estimating the model. Comparing model predictions with actual scalar magnetic field observations from the CHAMP satellite yields an rms misfit of 3.4 nT at non-polar latitudes and 5.4 nT at polar latitudes.

Key words: geomagnetic field, geomagnetic variation, inversion, spherical harmonics.

1 INTRODUCTION

The Ørsted satellite was launched on 1999 February 23 in a near-polar orbit with an inclination of 96.5°, a perigee at 640 km and an apogee at 880 km. The principal aim of the Ørsted mission (Olsen *et al.* 2000a; Neubert *et al.* 2001) is to accurately map the Earth's magnetic field, and high-precision magnetic field measurements spanning 2.5 yr are now available.

One of the first models derived from Ørsted data is now accepted as the IGRF 2000 (Olsen *et al.* 2000b), and data from geomagnetic quiet periods around 2000 January 1 were used to derive the *Ørsted Initial Field Model,* a snapshot of the geomagnetic field at epoch 2000 (Olsen *et al.* 2000a). The much extended and improved set of Ørsted data available now allows us to estimate the main field (the static part of the geomagnetic field) and its linear time change, the secular variation, with unprecedented accuracy.

However, in order to take full advantage of the improved data accuracy it is necessary to refine the usual way of deriving field models from satellite data. This paper describes the derivation of a model up to degree/order $N_{\mathrm{MF}} = 29$ for the core and low-degree crustal field and up to $N_{\mathrm{SV}} = 13$ for the secular variation. Special emphasis is laid on a correct statistical treatment of the data and on considering contributions from external current systems. Also investigated is the effect of including observatory data to constrain the secular variation part of the model.

It is now common practice in geomagnetic modelling to account for the time-varying magnetic field of the magnetospheric ring current (RC) by means of the *Dst* index (e.g. Langel 1987), which is derived from data of four ground-based observatories during all local times. However, satellite data used for field modelling are mostly taken from the nightside (to avoid contributions from ionospheric currents at middle and low latitudes), and the *Dst* index (which monitors only the symmetric part of the ring current) may not be a suitable measure of the perturbation that is observed by the satellite if the ring current is asymmetric. In addition, the final *Dst* index is not available for the most recent years, and therefore the provisional *Dst* index (see http://swdcdb.kugi.kyoto-u.ac.jp/) is often used instead. However, the provisional *Dst* index is known to be contaminated by baseline instabilities of the observatory data that were used for deriving the index. For these reasons a modified index,

$\widetilde{RC}$ (*cf.* Section 3.4), estimated from corrected data of observatories distributed worldwide in the same local-time sector as the satellite data, is used in this paper.

As opposed to this *deterministic* approach, which models the magnetic field of external sources, a *statistical* approach is used to account for ionospheric currents in the polar caps (dipole latitudes poleward of $\pm 75^\circ$). Their magnetic field behaviour is very difficult, if not impossible, to parametrize by indices. However, ionospheric conductivity during geomagnetic quiet conditions is mostly caused by photoionization by solar radiation, and therefore the effect of ionospheric polar cap currents is considered by allowing for larger residuals in sunlit areas (*cf.* Section 3.1).

2 DATA SELECTION

2.1 Satellite data

Ørsted scalar and vector data spanning 2.5 yr (1999 March–2001 September) were utilized. Data selection follows that used for the *Ørsted Initial Field Model* (Olsen *et al.* 2000a): the global index of geomagnetic activity $Kp \leq 1+$ for the time of observation and $Kp \leq 2$o for the previous 3 h interval; the index of magnetospheric ring-current strength, *Dst*, is within ± 10 nT and $|d(Dst)/dt| < 3$ nT hr^{-1}. The effect of polar cap ionospheric currents was minimized by excluding data from the polar caps for which the dawn–dusk component of the interplanetary magnetic field was $|B_y| > 3$ nT.

To reduce contributions from ionospheric currents at middle and low latitudes, only night-side data were used. The local time of the Ørsted orbit plane is slowly drifting; the local time T of the equator crossing of the south-going track decreases by 0.91 min d^{-1}, starting from an initial local time of 02:26 on 1999 February 23. This yields $T = 02{:}20$ (21:44, 19:00, 16:12, 13:28) at the beginning of 1999 March (2000 January; 2000 July; 2001 January; 2001 July). Owing to this drift, the south-going part of the orbit was used before 2000 July 1 (local time decreases from $T = 02{:}20$ to 19:00), whereas the north-going part was used in the second part of the mission (T decreases from 07:00 to 00:05 at the end of 2001 September). Analysis of the dawn–dusk Magsat data has shown that ionospheric currents are stronger during dusk compared with dawn (e.g. Langel *et al.* 1993), which is the reason for changing from a south-going to a north-going track when the local time was 07:00/19:00 rather than 06:00/18:00.

Vector data have been taken for dipole latitudes equatorward of $\pm 50^\circ$, scalar data were used for regions poleward of $\pm 50^\circ$ or if attitude data were not available. The data were decimated such that times of measurement were at least 60 s/sin θ apart, where the factor of sin θ (θ is the geographic colatitude) was used to simulate an equal-area distribution.

Compared with the data sets used for previous models such as the *Ørsted Initial Field Model,* all data have been recalibrated and a correction for stellar aberration (angular deflection owing to the finite value of the transverse relative speed compared with the speed of light) has been applied to the attitude information from the star imager (a correction of up to 20 arcsecs). Estimating models using uncorrected and corrected data, respectively, gave a lower misfit for the corrected data, indicating that the applied stellar aberration correction yields more consistent (vector) data.

2.2 Observatory data

In addition to the satellite data, measurements of secular variation at geomagnetic observatories were utilized. Data from 115 observatories were available for 1998, from 106 observatories for 1999, and from 94 observatories for the year 2000. Fig. 1 shows the distribution of these observatories.

Most authors use observatory annual means (e.g. Langel & Estes 1985b) or monthly means (e.g. Langlais & Mandea 2000) in addition to the satellite data to constrain secular variation. This is often combined with the estimation of observatory biases to account for the high-degree lithospheric field, as introduced by Langel *et al.* (1982). Estimation of observatory biases is not necessary if first time differences of the observatory data are used (e.g. Schmitz & Cain 1983; Cain *et al.* 1983). However, the usual annual (and monthly) means are calculated from all days (geomagnetic quiet and disturbed) and all local times (day and night data), and they are known to be contaminated by magnetic fields from ionospheric and magnetospheric current systems. Using local midnight data during geomagnetically quiet days results in less contaminated data (e.g. Olsen *et al.* 2002). For this reason (and for consistency with the selection procedure for the satellite data) a linear slope estimated from time-series of local midnight values during quiet periods (with the same criteria as for the satellite data) was estimated for each component and each observatory. This yields observatory estimates of $\dot{X}$, $\dot{Y}$ and $\dot{Z}$ for the first time derivative of the northward-, eastward- and downward-directed components of the magnetic field, respectively. Also estimated are

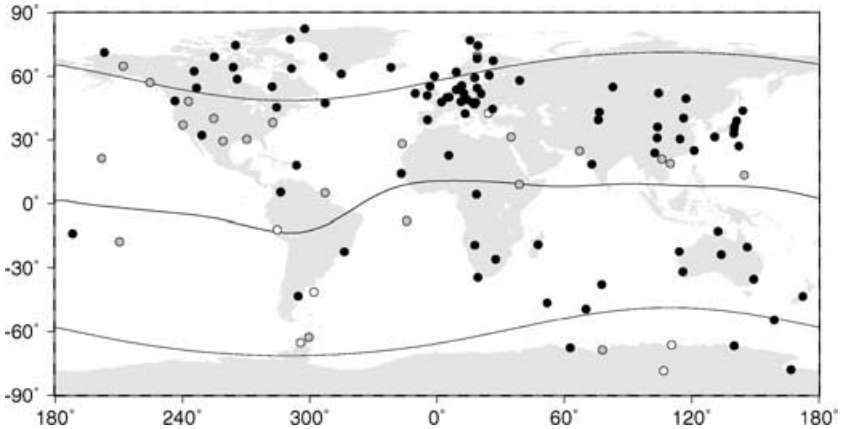

Figure 1. Distribution of observatories for the years 1998 (open circles), 1998–1999 (grey symbols) and 1998–2000 (black symbols), respectively. Also shown is the dip-equator and lines of $\pm 60^\circ$ dipole latitude.

the errors (standard deviation) of the slopes; typical values were between 0.4 and 0.9 nT yr^{-1}. After transformation from geodetic to geocentric components to obtain $\dot{B}_r$, $\dot{B}_\theta$ and $\dot{B}_\phi$ (and the corresponding errors $\sigma_{\dot{B}}$) these values were used to constrain the secular variation of the model. The effect of including these data is discussed in Section 4.

In addition, observatory hourly mean values were utilized to determine the strength of magnetospheric contributions, as described in Section 3.4.

3 MODEL PARAMETRIZATION AND ESTIMATION PROCEDURE

The magnetic field $\mathbf{B} = -\mathrm{grad}\, V$ is derived from a magnetic scalar potential V which is expanded in terms of spherical harmonics:

$$\begin{aligned} V = a\Bigg\{ & \sum_{n=1}^{N_{\mathrm{MF}}}\sum_{m=0}^{n}\left(g_n^m\cos m\phi + h_n^m \sin m\phi\right)\left(\frac{a}{r}\right)^{n+1} P_n^m(\cos\theta) \\ & + \sum_{n=1}^{N_{\mathrm{SV}}}\sum_{m=0}^{n}\left(\dot{g}_n^m\cos m\phi + \dot{h}_n^m \sin m\phi\right)(t-t_0)\left(\frac{a}{r}\right)^{n+1} \\ & \times P_n^m(\cos\theta) + \sum_{n=1}^{2}\sum_{m=0}^{n}\left(q_n^m\cos m\phi + s_n^m\sin m\phi\right) \\ & \times \left(\frac{r}{a}\right)^n P_n^m(\cos\theta) + \widetilde{RC}\left[\left(\frac{r}{a}\right) + Q_1\left(\frac{a}{r}\right)^2\right] \\ & \times \left[\tilde{q}_1^0 P_1^0(\cos\theta) + \left(\tilde{q}_1^1\cos\phi + \tilde{s}_1^1\sin\phi\right)P_1^1(\cos\theta)\right]\Bigg\}. \end{aligned} \quad (1)$$

$a = 6371.2$ km is the mean radius of the Earth, (r, θ, ϕ) are geocentric spherical coordinates, $P_n^m(\cos\theta)$ are the associated Schmidt semi-normalized Legendre functions of degree n and order m, and (g_n^m, h_n^m) and (q_n^m, s_n^m) are the Gauss coefficients describing sources internal and external to the Earth, respectively. $(\dot{g}_n^m, \dot{h}_n^m)$ describe the (linear) secular variation around model epoch t_0, which is chosen to be 2000.0 in this paper. In addition, the $n = 1, 2$, $m = 0$, terms incorporated an annual and semi-annual variation, as described below. The last part of the above equation (coefficients $\tilde{q}_1^0$, $\tilde{q}_1^1$ and $\tilde{s}_1^1$) accounts for the variability of contributions from the magnetospheric ring current (as measured by $\widetilde{RC}$, defined in Section 3.4) plus their internal, induced counterpart. These induced contributions are considered by means of the factor $Q_1 = 0.27$, a value found by Langel & Estes (1985a).

Experiments with various truncation levels N_{MF} of the main field show that the magnetic power R_n increases for $n > 26$, and that of the secular variation increases for $n > 11$. To reduce contamination of the lower-degree expansion coefficients by spatial aliasing, the analysis was performed up to $N_{\mathrm{MF}} = 29$ for the main field and up to $N_{\mathrm{SV}} = 13$ for the secular variation. However, coefficients above degree 25 for the main field and above degree 11 for the secular variation are probably not robust.

Previous model versions show that external contributions contain a considerable seasonal variation. This concerns mostly the zonal coefficients ($m = 0$), and therefore q_1^0 and q_2^0 (and the corresponding internal coefficients g_1^0 and g_2^0) are allowed to vary with annual and semi-annual periodicity according to

$$\begin{aligned} q_n^0(\tau) = q_{n,0}^0 & + \left(q_{n,1c}^0\cos\tau + q_{n,1s}^0\sin\tau\right) \\ & + \left(q_{n,2c}^0\cos 2\tau + q_{n,2s}^0\sin 2\tau\right) \end{aligned} \quad (2)$$

(and similar for g_n^0) for $n = 1$ and 2, where τ is season (starting on January 1) in radians.

All data points are collected in the data vector $\mathbf{d}_{\mathrm{obs}} = (\mathbf{d}_{\mathrm{vector,sat}}^{\mathrm{T}}, \mathbf{d}_{\mathrm{scalar,sat}}^{\mathrm{T}}, \mathbf{d}_{\mathrm{obs}}^{\mathrm{T}})^{\mathrm{T}}$, which consists of a first part $\mathbf{d}_{\mathrm{vector,sat}} = (B_{r,1}, B_{\theta,1}, B_{\phi,1}, \ldots, B_{r,N_{\mathrm{vector}}}, B_{\theta,N_{\mathrm{vector}}}, B_{\phi,N_{\mathrm{vector}}})^{\mathrm{T}}$ of length $3N_{\mathrm{vector}}$ with the satellite vector triplets, a second part, $\mathbf{d}_{\mathrm{scalar,sat}} = (F_1, \ldots, F_{N_{\mathrm{scalar}}})^{\mathrm{T}}$ of length N_{scalar} containing the satellite scalar observations and a third part $\mathbf{d}_{\mathrm{obs}} = (\dot{B}_{r,1}, \dot{B}_{\theta,1}, \dot{B}_{\phi,1}, \ldots, \dot{B}_{r,N_{\mathrm{obs}}}, \dot{B}_{\theta,N_{\mathrm{obs}}}, \dot{B}_{\phi,N_{\mathrm{obs}}})^{\mathrm{T}}$ of length $3N_{\mathrm{obs}}$ with the observatory values of secular variation. Likewise, the 1121 model parameters of eq. (1) (899 static internal coefficients, 195 internal coefficients of secular variation, eight static external coefficients, three coefficients of $\widetilde{RC}$ dependence, 16 coefficients of seasonal variation) are collected in the model vector $\mathbf{m}$.

These coefficients are estimated by the *Iteratively Reweighted Least-Squares* (IRLS) approach, minimizing the chi-squared misfit $\mathbf{e}^{\mathrm{T}}\underline{\underline{\mathbf{C}}}^{-1}\mathbf{e}$, where $\underline{\underline{\mathbf{C}}}$ is the data error covariance matrix and the residuals $\mathbf{e} = \mathbf{d}_{\mathrm{obs}} - \mathbf{d}_{\mathrm{mod}}$ are given by the difference of observations (data vector $\mathbf{d}_{\mathrm{obs}}$) and values $\mathbf{d}_{\mathrm{mod}}$ predicted by the model. The estimated model vector of the ith iteration may be written as

$$\mathbf{m}_{i+1} = \mathbf{m}_i + \delta\mathbf{m}_i$$

$$\delta\mathbf{m}_i = \left[\underline{\underline{\mathbf{G}}}_i^{\mathrm{T}}\cdot\underline{\underline{\mathbf{C}}}^{-1}\cdot\underline{\underline{\mathbf{G}}}_i\right]^{-1}\left[\underline{\underline{\mathbf{G}}}_i^{\mathrm{T}}\cdot\underline{\underline{\mathbf{C}}}^{-1}\cdot(\mathbf{d}_{\mathrm{obs}}-\mathbf{d}_{\mathrm{mod}})\right]$$

with

$$\underline{\underline{\mathbf{G}}}_i = \left.\frac{\partial\mathbf{d}_{\mathrm{mod}}(\mathbf{m})}{\partial\mathbf{m}}\right|_{\mathbf{m}=\mathbf{m}_i}$$

and $\underline{\underline{\mathbf{G}}}_i^{\mathrm{T}}$ as the transpose of $\underline{\underline{\mathbf{G}}}_i$. If the data errors were uncorrelated and Gaussian distributed with variance σ^2, choosing $\underline{\underline{\mathbf{C}}}^{-1}$ as a diagonal matrix with elements $1/\sigma^2$ would yield the best model estimate in the maximum-likelihood sense.

Real data, however, are often not Gaussian distributed, and may be correlated. Previous modelling efforts have demonstrated that the Ørsted data are correlated (e.g. Holme 2000). The construction of the data covariance matrix that matches the statistical properties of the data is critical for obtaining good models. In this study, a covariance matrix is used that accounts for: (1) correlated noise caused by attitude errors; (2) ionospheric current contributions in sunlit areas; and (3) non-Gaussian data errors, for instance caused by outliers.

3.1 Considering attitude errors and contributions from ionospheric polar cap currents

To account for the anisotropy in the attitude accuracy of Ørsted the correlated data covariance matrix given by Holme & Bloxham (1996) was used. The attitude uncertainty results in non-vanishing covariances in the noise of B_r, B_ϑ and B_ϕ. However, the magnetic field components can be transformed into a new coordinate system in which the components are uncorrelated.

Let $\hat{\mathbf{n}}$ be the unit vector of the bore-sight of the star imager, and let $\mathbf{B}$ be the observed magnetic field vector. The magnetic residual vector

$$(\delta B_B, \delta B_\perp, \delta B_3)^{\mathrm{T}} = \underline{\underline{A}}\cdot(\delta B_r, \delta B_\vartheta, \delta B_\phi)^{\mathrm{T}} \quad (3)$$

is transformed such that the first component, δB_B, is in the direction of $\mathbf{B}$, the second component, $\delta B_\perp$, is aligned with $(\hat{\mathbf{n}}\times\mathbf{B})$ and the third component, δB_3, is aligned with $\mathbf{B}\times(\hat{\mathbf{n}}\times\mathbf{B})$. In that coordinate system the data covariance matrix is a diagonal matrix with elements $(\sigma_B^2, \sigma_\perp^2, \sigma_3^2)$, where $\sigma_\perp^2 = \sigma_B^2 + (\hat{\mathbf{n}}\times\mathbf{B})\chi^2 + (\hat{\mathbf{n}}\cdot\mathbf{B})\psi^2$ and

$\sigma_3^2 = \sigma_B^2 + B^2\psi^2$. ψ is the standard deviation of the bore-sight direction (pointing error), χ is that of the angle around the bore-sight (rotation error) and σ_B is the (attitude-independent) standard deviation of the scalar intensity. For the present model we used a pointing uncertainty of $\psi = 10$ arcsec, a rotation uncertainty of $\chi = 60$ arcsec (this value is decreased to $\chi = 40$ arcsec for data after 2000 January 22, owing to improvements in the Ørsted star imager parameter settings), and a scalar uncertainty σ_B as defined below. A data covariance matrix defined by these numbers corresponds to a downweighting of the less accurate $B_\perp$-component.

Ionospheric currents are of internal origin as seen by the satellite, and may therefore contaminate the internal field coefficients. To account for their magnetic perturbations, larger residuals are allowed in sunlit (i.e. summer polar) areas where the ionospheric conductivity, caused partly by solar irradiation, is higher and hence stronger ionospheric currents may occur. If photoionization is the dominant process (as is the case during geomagnetically quiet conditions), ionospheric conductivity varies with the zenith angle κ of the Sun as $\sqrt{\cos\kappa}$ (Schlegel 1988; Stauning & Primdahl 2000). Taking this dependence as a guideline, it has been decided to vary the scalar data error σ_B with κ according to $\sigma_B^2 = (3\ \mathrm{nT})^2 + (15\ \mathrm{nT})^2 \cos\kappa$. For the data used in this study $\cos\kappa$ varies between 0 and 0.45, which increases σ_B from 3 nT (dark areas) to 10.5 nT (at the summer pole). However, very little is known concerning the statistics of polar ionospheric contributions during geomagnetic quiet periods, and therefore this parametrization should be regarded as an *ad hoc* choice; other values of the parameters and a different functional dependence may work as well.

3.2 Robust model estimation and the Iteratively Reweighted Least-Squares method

Correct application of the least-squares method (in the maximum-likelihood sense) requires Gaussian distributed data errors. This, however, is often not the case. Walker & Jackson (2000) (see also Bloxham *et al.* 1989) demonstrate that some magnetic data, for instance historical observations of declination, follow a Laplace distribution rather than a Gaussian distribution. The Ørsted residuals are also not Gaussian distributed. As shown in Section 4, the actual distribution is better described by a *Huber distribution* (Gaussian distribution in the centre ($\sigma < 1.5$), Laplace distribution in the tails). Data with a non-Gaussian error distribution can be treated by means of the *Iteratively Reweighted Least Squares* method; see Huber (1964); Hogg (1979); Constable (1988); Walker & Jackson (2000) for a description of this approach.

In IRLS each data point is weighted according to its standard deviation σ_k and according to the size of its residual with respect to the model. Here we use *Huber weights*

$$w_{k,i} = \max(c/\varepsilon_{k,i}, 1) \tag{4}$$

with $c = 1.5$ and $\varepsilon_{k,i} = (d_{\mathrm{obs},k} - d^{(i)}_{\mathrm{mod},k})/\sigma_k$ as the normalized residual of the kth data point in the ith iteration. These weights are collected in the diagonal weight matrix $\underline{\underline{\mathbf{W}}}_i$. As demonstrated, for instance, by Constable (1988), IRLS with Huber weights corresponds to a maximum-likelihood estimation if the data errors were distributed according to a Huber distribution

$$h(\varepsilon) = \frac{1}{N}\begin{cases}\exp(-\varepsilon^2/2) & |\varepsilon| < c\\ \exp(-c|\varepsilon| + c/2) & |\varepsilon| \geq c,\end{cases} \tag{5}$$

where the normalization factor $N = 2.6046$ (for $c = 1.5$) is found from $\int_{-\infty}^{\infty} h(\varepsilon)\,d\varepsilon = 1$.

Table 1. Numbers of data points, N, means and rms misfits (in nT or nT yr^{-1}) for the different components. 'Polar' denotes data poleward of 50° dipole latitude. The quantity η indicates how much the component contributes to the model (see text).

Component	N	Mean	rms	η (per cent)
F_{polar}	14 036	−0.36	4.76	20
$F_{\mathrm{non\text{-}polar}} + B_B$	54 412	0.02	2.89	51
$B_\perp$	24 585	0.13	6.40	8
B_3	24 585	0.15	3.25	19
$\dot{B}_{r,\mathrm{obs}}$	119	−1.26	5.09	
$\dot{B}_{\theta,\mathrm{obs}}$	119	2.99	5.77	2
$\dot{B}_{\phi,\mathrm{obs}}$	119	0.06	4.70	

3.3 The combined data covariance matrix

As pointed out by Walker & Jackson (2000), two iterative procedures are generally invoked in robust geomagnetic field modelling: one owing to the use of non-linear magnetic data (such as the scalar intensity) and the other owing to the dependence of the robust weights $w_{k,i}$ on the residuals. Following Farquharson & Oldenburg (1998) and Walker & Jackson (2000), these two procedures can be combined by constructing the inverse of the data covariance matrix of the ith iteration:

$$\underline{\underline{\mathbf{C}}}_i^{-1} = \underline{\underline{\mathbf{A}}}^{\mathrm{T}}\,\underline{\underline{\mathbf{S}}}^{\mathrm{T}}\,\underline{\underline{\mathbf{W}}}_i\,\underline{\underline{\mathbf{S}}}\,\underline{\underline{\mathbf{A}}} \tag{6}$$

with $\underline{\underline{\mathbf{A}}}$ from eq. (3) and $\underline{\underline{\mathbf{S}}} = \mathrm{diag}\{1/\sigma_B, \ldots, 1/\sigma_\perp, \ldots, 1/\sigma_3\}$.

$\underline{\underline{\mathbf{C}}}_i^{-1}$ defined thus describes only the covariances of the Ørsted vector data; before applying to the whole data vector $\mathbf{d}_{\mathrm{obs}}$ it has to be augmented with the diagonal elements $w_{k,i}/\sigma_B^2$ that correspond to the Ørsted scalar observations and with the diagonal elements $w_{k,i}/\sigma_{\mathrm{obs}}^2$ that correspond to the observatory values. The value of σ_{obs} is different for each observatory and component, and was chosen as $\sigma_{\mathrm{obs}} = 5\sigma_{\dot{B}}$, with $\sigma_{\dot{B}}$ as the standard deviation of the slope defined in Section 2.2. This calibration of the error assigned to the observatory data was necessary because the *a posteriori* misfit (*cf.* Table 1) is about five times as large as the typical error $\sigma_{\dot{B}}$. Note that $\underline{\underline{\mathbf{C}}}_i^{-1}$ is different for each iteration owing to the dependence of the robust weight matrix $\underline{\underline{\mathbf{W}}}_i$ on the residuals of the previous iteration, which is the reason for denoting the approach as *iteratively reweighted least-squares*.

Four iterations were found to be sufficient for convergence. Gross outliers (residuals with $\epsilon > 5$) were removed in the second to last iteration.

3.4 Modelling contributions from the magnetospheric ring current

Traditionally, the *Dst* index is used in geomagnetic field modelling as a measure of the magnetospheric ring current for data selection as well as for accounting for the magnetic field of the RC. However, *Dst* measures only the axially symmetric ring current, and the field perturbation on the Earth's night-side, from where data for field modelling are typically taken, may differ from that given by *Dst*. In addition, the final *Dst* index becomes available only after several years, and the baseline of the provisional *Dst* index is known to be unstable. To overcome these difficulties, data from geomagnetic observatories distributed worldwide on the night-side were used to derive a modified index, denoted as $\widetilde{RC}$. Using this index instead of *Dst* improved the fit to the data considerably, especially for data

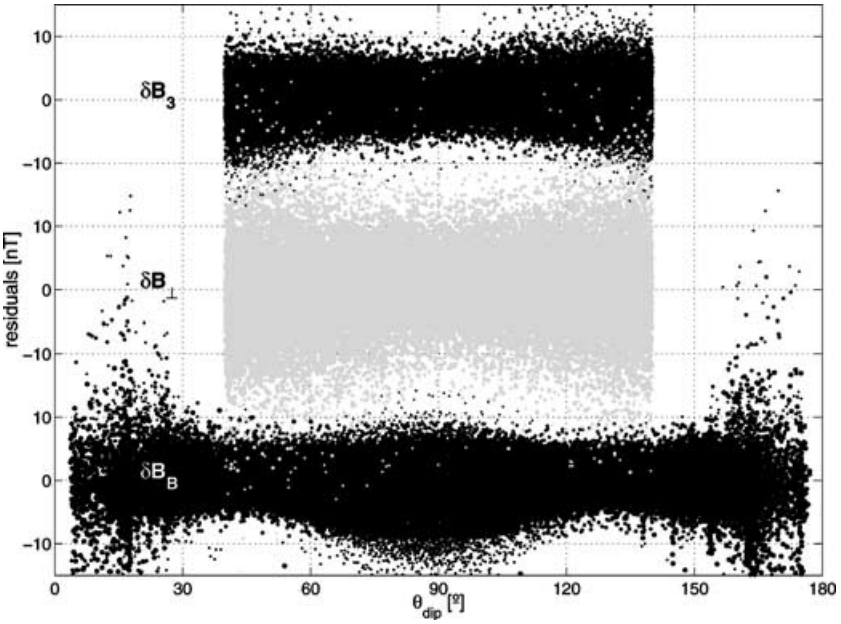

Figure 2. Model residuals as a function of dipole colatitude $\theta_{\rm dip}$. The symbol size is proportional to the data weight w.

periods after 1999 December 31 for which only the provisional *Dst* index (and not the final index) was available.

$\widetilde{RC}$ is determined in the following way: hourly mean values of observatories equatorward of $\pm 60^\circ$ dipole latitudes are used, and a baseline, defined by the linear slope derived in Section 2.2, is subtracted from the data of each component and each observatory. The horizontal components are rotated from geographic to geomagnetic components; $\Delta X_{\rm dip}$ is the residual in the direction of the geomagnetic north pole. Finally, for each hour, $dP_1^0/d\theta_{\rm dip} = -\sin\theta_{\rm dip}$ ($\theta_{\rm dip}$ is the dipole colatitude) is fitted to $\Delta X_{\rm dip}$, and $\widetilde{RC}$ is defined as the amplitude of that term. Observatories at local midnight are given maximum weight, $w = 1$; the weights decrease toward dawn/dusk according to $\max(\cos T/2, 0)$, where T is the local time (in radians). Owing to the uneven spatial distribution of observatories, the (weighted) number of observatories varies between $\sum w = 13.0$ at $UT = 8$ and $\sum w = 48.7$ at $UT = 20$.

Unfortunately, sufficient observatory hourly mean values were not available for 2001, and therefore the provisional *Dst* index instead of $\widetilde{RC}$ was used for 2001. A comparison of the different indices for the year 1999 revealed baseline instabilities (of up to ± 10 nT) in the provisional *Dst* index, especially around 1999 September 1; it turns out that there is better agreement between $\widetilde{RC}$ and the final *Dst* index compared with the provisional *Dst* index, especially concerning the baseline. It must be assumed that the provisional *Dst* index for 2001 that is used in this study is also affected by baseline instabilities; indications for this will be presented below.

4 RESULTS AND DISCUSSION

The number of data points used, residual means and rms misfits of the model are given in Table 1. The mean values are close to zero for all components. This is an improvement compared with the *Ørsted Initial Field Model* (for which the mean of $\delta B_\perp$ was as high as 1.2 nT) and is a result of recalibration and correction for stellar aberration effects of the data used in the present study.

Both $\delta B_\perp$ and δB_3 are residual components perpendicular to the magnetic field; the twofold larger scatter of $\delta B_\perp$ (6.4 nT rms) compared with δB_3 (3.2 nT rms) is caused by the anisotropic accuracy of the Ørsted star imager and confirms the necessity of downweighting the $B_\perp$ component. η of Table 1 indicates how much the various components contribute to the model and was found from a resolution analysis (Tarantola 1987). The scalar data ($F + B_B$) constrains 71 per cent of the total number of model parameters, the vector component B_3 constrains 19 per cent, whereas the less accurate vector component $B_\perp$ constrains only 8 per cent. The observatory data (which contributes only to the secular variation part of the model) constrains the remaining 2 per cent of the model parameters.

Fig. 2 shows the data residuals (δB_B, $\delta B_\perp$, δB_3) as a function of dipole colatitude $\theta_{\rm dip}$ (in this and the following figures δB_B denotes the scalar residual of scalar as well as vector data and therefore includes δF). The minimum scatter of the scalar residuals δB_B near $\pm 35^\circ$ dipole latitude (corresponding to $\theta_{\rm dip} = 55^\circ$ and 125°, respectively) and its maximum at the equator and at polar latitudes indicate unmodelled contributions from the magnetospheric ring current (a ring current in the equatorial plane of a purely dipolar main field produces a magnetic field that is perpendicular to the main field at $\pm 35^\circ$ dipole latitude, thereby not contributing to the scalar residuals at those latitudes). This is confirmed by Fig. 3, which shows δB_B for the year 1999 when $\widetilde{RC}$ (top) or the (final) *Dst* index (bottom), respectively, are used when estimating the model to account for the magnetic effect of the ring current. Using $\widetilde{RC}$ results in considerably less scatter at low latitudes (2.34 nT rms for dipole latitudes equatorwards of $\pm 20^\circ$) compared with using *Dst* (3.06 nT).

Fig. 4 shows the residuals as a function of time. The absence of vector data between 2000 May and November is a result of thermal problems when the satellite was in a dawn–dusk orbit. The scatter of $\delta B_\perp$ is reduced after 2000 January 22 (day count 20, the dotted vertical line) owing to improved parameter settings of the Ørsted star imager, resulting in an rms misfit of 7.88 and 5.77 nT before and after that date, respectively. δB_B for dipole latitudes equatorwards of $\pm 50^\circ$ are shown by black symbols, whereas those for polar latitudes are shown by grey symbols. Note the jumps of the non-polar scalar

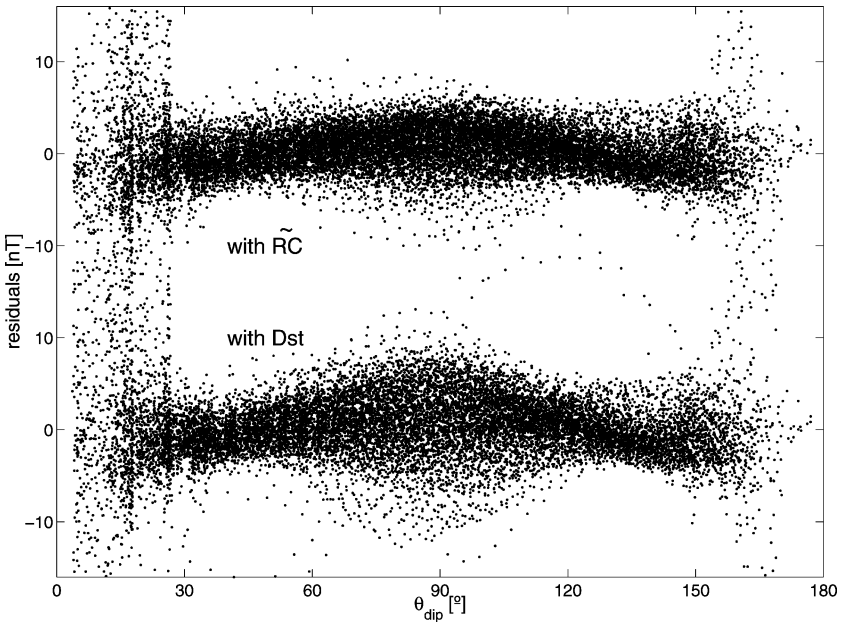

Figure 3. δB_B for 1999 as a function of dipole colatitude if $\widetilde{RC}$ (top) or *Dst* (bottom), respectively, is used to account for the magnetic effect of the ring current.

residuals around day count 480 (2001 April 25) and after day count 570 (2001 July 24). These are probably caused by baseline instabilities in the provisional *Dst* index (that has been used to account for external sources), as will be discussed below.

Fig. 5 presents normal probability plots of the residuals ε. Also shown are theoretical curves for a Gaussian distribution (straight line) and for a Huber distribution with $c = 1.5$ (S-shaped curve). It is clearly seen that the residuals do not follow a Gaussian distribution. The actual distributions are closer to a Huber distribution, thus confirming the use of *IRLS* with Huber weights. This is true for all components except for scalar residuals. The distribution of δF_{polar} is asymmetric: it is close to a Huber distribution for negative residuals, but positive $\varepsilon > +2$ are more frequent than negative residuals $\varepsilon < -2$. For non-polar latitudes, negative residuals of δB_B are more frequent than positive residuals, which is probably caused by an inadequate description of the ring-current variability. All of this indicates the need for improved models of external source contributions.

Table 2 lists the static external coefficients q_n^m and s_n^m, the external coefficients $\tilde{q}_n^m$ and $\tilde{s}_n^m$ that depend on the strength of the ring current, and the annual and semi-annual terms of the coefficients q_n^0 and g_n^0. By far the largest external term is q_1^0. Static external coefficients for $n > 1$ are negligibly small; however, q_2^0 shows a pronounced annual variation. This is in agreement with the value $q_2^0 = 1.57$ nT of

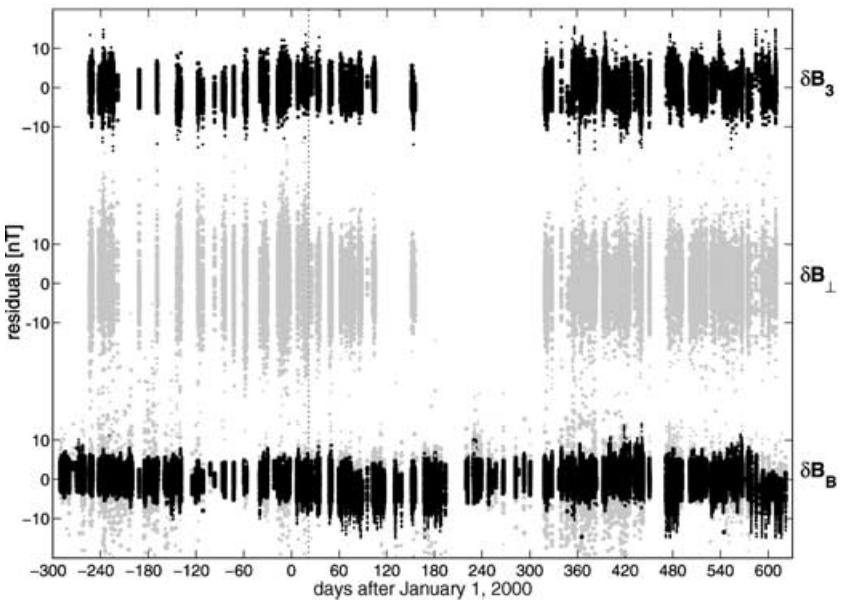

Figure 4. Same as in Fig. 2, but versus time. δB_B for dipole latitudes equatorwards of 50° is shown by black symbols, whereas the polar latitude δB_B is shown by grey symbols.

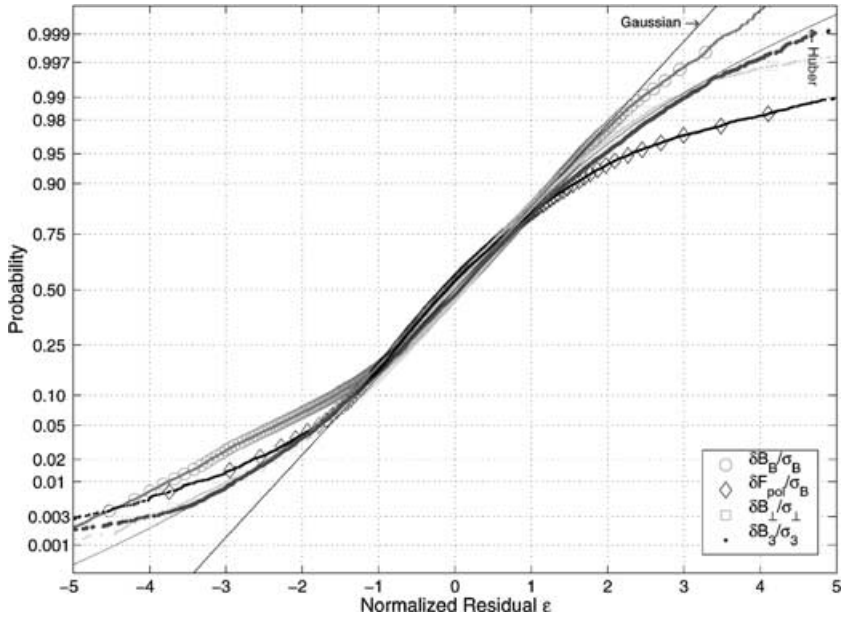

Figure 5. Normal probability plots of the residuals ε. Also shown are theoretical curves for a Gaussian distribution (straight line) and for a Huber distribution with $c = 1.5$ (S-shaped curve).

the *Ørsted Initial Field Model,* which was derived from winter data only.

These seasonal terms can be explained, at least qualitatively, by seasonal movement of part of the magnetospheric ring current with respect to the equatorial plane (Malin & Mete Isikara 1976). This movement produces an annual variation (with a maximum during solstices) of symmetric terms such as q_2^0, and a semi-annual variation (with a maximum during equinoxes) of asymmetric terms such as q_1^0. If internal coefficients were entirely induced, and if the Earth's conductivity were independent of latitude and longitude (1-D conductivity), then each external coefficient would induce only one internal coefficient of the same degree and order. From typical values of mantle conductivity one would expect ratios $Q_n = g_n^0/q_n^0$ of $Q_1 = 0.17$, $Q_2 = 0.11$ for the annual variation, and of $Q_1 = 0.21$ and $Q_2 = 0.15$ for the semi-annual variation. However, the values of Table 2 do not follow such a simple relation. This could be a result of the existence of sources internal to the satellite orbit (short-period secular variation, or ionospheric sources, for instance) with periods of 6 and 12 months that are not induced purely by the external (magnetospheric) sources.

The inclusion of ground-based secular variation information yields an improved description of the observatory data, at the cost of almost no increase of the satellite misfit. This is shown in Table 3, which compares the present model (A) with a model (B) that is similar to Model A except that it was derived without observatory data. The difference in satellite misfit between the two models is below 0.01 nT; however, there is considerable improvement in the fit of the observatory data, especially in $\dot{B}_r$.

How well can the models explain magnetic data that were not used for their derivation? To answer this question scalar data from the recently launched CHAMP satellite were selected using the same criteria as for the Ørsted data. The resulting set of test data consists of 6462 measurements sampled between 2000 August and December at altitudes of about 450 km. There are 1571 data points at polar latitudes and 4891 at non-polar latitudes. The result of this comparison (using $\widetilde{RC}$ for describing magnetospheric sources) is shown in the lower part of Table 3. Although obtained with a different instrument and at a different altitude, the low mean value of 0.1 nT at low latitudes indicates the high compatibility of the Ørsted and CHAMP data and confirms the excellent data quality. Visual inspection of the latitudinal dependence of the residuals shows that the largest residuals occur at polar latitudes. Their size is somewhat larger than the polar Ørsted residuals owing to the lower altitude of CHAMP compared with Ørsted, which puts CHAMP closer to ionospheric currents.

However, there are also significant residuals at low latitudes caused by the part of the crustal field that is not modelled with spherical harmonic degrees $n \leq 29$, for instance over Middle and West-Africa (the Bangui anomaly). The low altitude makes CHAMP ideal for studying crustal fields, and recently Maus *et al.* (2002) derived a first map of the crustal field from CHAMP scalar data after subtraction of the field model presented here.

Table 2. Expansion coefficients of external contributions (q_n^m, s_n^m), in nT. $\tilde{q}_n^m$ and $\tilde{s}_n^m$ present the $\widetilde{RC}$-dependent part of the external coefficients. Also shown are the terms describing the seasonal variation of q_n^0, in nT.

n	m	Static		*Dst*-dependent		Annual				Semi-annual			
		q_n^m	s_n^m	$\tilde{q}_n^m$	$\tilde{s}_n^m$	$q_{n,1c}^0$	$q_{n,1s}^0$	$g_{n,1c}^0$	$g_{n,1s}^0$	$q_{n,2c}^0$	$q_{n,2s}^0$	$g_{n,2c}^0$	$g_{n,2s}^0$
1	0	24.00	—	−0.64	—	−0.86	−1.33	−0.89	0.60	−1.41	−2.07	0.66	0.52
1	1	0.73	−3.32	−0.01	0.09	—	—	—	—	—	—	—	—
2	0	0.06	—	—	—	1.84	−0.04	0.40	−0.26	0.03	0.13	−0.47	0.05
2	1	−0.07	0.15	—	—	—	—	—	—	—	—	—	—
2	2	−0.11	0.09	—	—	—	—	—	—	—	—	—	—

Table 3. Top: mean and rms misfit (in nT yr^{-1}) to the observatory secular variation data if these data are included (Model A) or excluded (Model B) when estimating the model. Bottom: mean and rms misfit (in nT) between predictions of the models and CHAMP scalar observations.

	Model A		Model B	
	Mean	rms	Mean	rms
$\dot{B}_r$	−1.26	5.09	−2.22	7.32
$\dot{B}_\theta$	2.99	5.77	3.75	6.49
$\dot{B}_\phi$	0.06	4.70	0.37	5.21
$F_{\mathrm{CHAMP,polar}}$	0.97	5.36	0.99	5.37
$F_{\mathrm{CHAMP,non\text{-}polar}}$	0.09	3.41	0.11	3.41

Other model parametrizations and estimation techniques have been tried during the preparation of this model (for instance: robust versus non-robust estimation, use of *Dst* instead of $\widetilde{RC}$, no down-weighting of data in sunlit areas, a different truncation level for the external and seasonal variations). All models were evaluated based on their rms misfit, and on the misfit between model predictions and CHAMP observations. Although the differences of model misfits are often rather small (for instance, the difference of misfit to CHAMP data for the two models presented in Table 3), the model presented here yields the lowest overall misfit.

Finally, CHAMP scalar data for 2001 were used to study the peculiar time variability of the low-latitude Ørsted scalar residuals for 2001 that are shown in Fig. 4; for instance, around day count 480 and after day count 570. It turns out that similar jumps and excursions are seen in the CHAMP residuals (after accounting for magnetospheric sources using the provisional *Dst* index), indicating that both Ørsted and CHAMP observe coherently magnetospheric ring current signatures that are not monitored by the provisional *Dst* index.

5 CONCLUSIONS

The presented model describes the static part of the geomagnetic field (up to degree/order 29) and its linear time change (up to degree/order 13) for epoch 2000.0. It is an improvement of the *Ørsted Initial Field Model,* using more and better data, and new techniques for model parametrization and model estimation.

The model coefficients are available at www.dsri.dk/Oersted/Field_models/OSVM/; however, main field coefficients with $n > 25$ and secular variation coefficients with $n > 11$ are probably not robust. The rms misfit to the scalar data that were used when deriving the model is 2.9 nT at non-polar latitudes, and comparing model predictions with actual scalar measurements from the CHAMP satellite (which were not used when deriving the model) yields an rms misfit of 3.4 nT at non-polar latitudes and of 5.4 nT at polar latitudes.

For Gaussian-distributed noise one would expect 0.27 per cent of the residuals to have magnitude $>3\sigma$; however, the actual number is about 3 times higher, indicating a long-tailed distribution of the data errors. The *a posteriori* probability density of the residuals indicate that the actual distributions are more similar to a Huber distribution than to a Gaussian distribution, thus confirming the use of the *iteratively reweighted least-squares* method with Huber weights when estimating the model.

Ionospheric currents at polar latitudes are almost always present, though of extremely varying amplitudes. An attempt to consider these currents in a statistical way by allowing for larger residuals in sunlit (summer polar) areas (where the ionospheric conductivity, caused mainly by solar irradiation, is higher) was only partially successful. This approach has a positive effect on the model (as indicated by the model misfit and by the ability of the model to predict CHAMP observations); however, it turns out that the distribution of the magnetic field contributions to the scalar field is asymmetric (positive values are much more frequent than negative values of similar amplitude), and more advanced models of the statistical properties of ionospheric currents are needed to account for their influence on field models.

In contrast to most previous models, external terms up to $n = 2$ are included in the model, the zonal term of which shows a prominent annual variation of 1.8 nT amplitude. Time-varying contributions from the magnetospheric ring current are successfully described by an index (called $\widetilde{RC}$) derived from simultaneous hourly mean values of geomagnetic observatories in the same local time sector as the satellite. Using this index results in better agreement with the satellite observations compared with *Dst*. This indicates that one of the limiting factors in field modelling with data from high-precision geomagnetic satellites such as Ørsted, CHAMP and Ørsted-2/SAC-C is the availability of a suitable indicator of magnetospheric field contributions for the same time instant and geographic longitude as the satellite data.

ACKNOWLEDGMENTS

I wish to thank David Barraclough, Richard Holme, Gauthier Hulot, Frank Lowes, Mike Purucker and Terry Sabaka for suggestions and helpful discussions. The Ørsted Project was made possible by extensive support from the Ministry of Trade and Industry, the Ministry of Research and Information Technology and the Ministry of Transport in Denmark. Additional international and crucial support were provided by NASA, ESA, CNES and DARA. I would like to thank Hermann Lühr, PI of the CHAMP Magnetic Field Investigation, for providing the CHAMP scalar magnetic field data. The CHAMP satellite project is supported by grants from the German Space Agency (DLR) under contract FKZ 50 EP 9587.

REFERENCES

Bloxham, J., Gubbins, D. & Jackson, A., 1989. Geomagnetic secular variation, *Phil. Trans. R. Soc. Lond.,* A., **329,** 415–502.

Cain, J.C., Frayser, J., Muth, L. & Schmitz, D., 1983. The use of MAGSAT data to determine secular variation, *J. geophys. Res.,* **88,** 5903–5910.

Constable, C.G., 1988. Parameter estimation in non-Gaussian noise, *Geophys. J.,* **94,** 131–142.

Farquharson, C.G. & Oldenburg, D.W., 1998. Non-linear inversion using general measures of data misfit and model structure, *Geophys. J. Int.* **134,** 213–227.

Hogg, R.V., 1979. An introduction to robust estimation, in *Robustness in Statistics,* pp. 1–17, eds Launer, R.L. & Wilkinson, G.N., Academic Press, San Diego, CA.

Holme, R., 2000. Modelling of attitude error in vector magnetic data: application to Ørsted data, *Earth, Planets, Space,* **52,** 1187–1197.

Holme, R. & Bloxham, J., 1996. The treatment of attitude errors in satellite geomagnetic data, *Phys. Earth planet. Inter.,* **98,** 221–233.

Huber, P.J., 1964. Robust estimation of a location parameter, *Ann. Math. Statist.,* **35,** 73–101.

Langel, R.A., 1987. The main field, in, *Geomagnetism,* Vol. 1, pp. 249–512, ed. Jacobs, J.A., Academic Press, London.

Langel, R.A. & Estes, R.H., 1985a. Large-scale, near-Earth magnetic fields from external sources and the corresponding induced internal field, *J. geophys. Res.,* **90,** 2487–2494.

Langel, R.A. & Estes, R.H., 1985b. The near-Earth magnetic field at 1980 determined from MAGSAT data, *J. geophys. Res.,* **90,** 2495–2509.

Langel, R.A., Estes, R.H. & Mead, G.D., 1982. Some new methods in geomagnetic field modelling applied to the 1960–1980 epoch, *J. Geomag. Geoelectr.,* **34,** 327–349.

Langel, R.A., Purucker, M. & Rajaram, M., 1993. The equatorial electrojet and associated currents as seen in MAGSAT data, *J. Atmos. Terr. Phys.,* **55,** 1233–1269.

Langlais, B. & Mandea, M., 2000. An IGRF candidate main geomagnetic field model for epoch 2000 and a secular variation model for 2000–2005, *Earth, Planets, Space,* **52,** 1137–1148.

Malin, S.R.C. & Mete Isikara, A., 1976. Annual variation of the geomagnetic field, *Geophys. J. R. astr. Soc.,* **47,** 445–457.

Maus, S., Rother, M., Holme, R., Lühr, H., Olsen, N. & Haak, V., 2002. First CHAMP satellite magnetic data resolve uncertainty about strength of the lithospheric magnetic field, *Geophys. Res. Lett.,* in press.

Neubert, T. *et al.,* 2001. Ørsted satellite captures high-precision geomagnetic field data, *EOS, Trans. Am. geophys. Un.,* **82,** 81–88.

Olsen, N. *et al.,* 2000a. Ørsted initial field model, *Geophys. Res. Lett.,* **27,** 3607–3610.

Olsen, N., Sabaka, T.J. & Tøffner-Clausen, L., 2000b. Determination of the IGRF 2000 model, *Earth, Planets, Space,* **52,** 1175–1182.

Olsen, N., Moretto, T. & Friis-Christensen, E., 2002. New approaches to explore the Earth's magnetic field, *J. Geodyn.,* **32,** 29–41.

Schlegel, K., 1988. Auroral zone E-region conductivities during solar minimum derived from EISCAT data, *Ann. Geophys.,* **6,** 129–138.

Schmitz, D.R. & Cain, J.C., 1983. Geomagnetic spherical harmonic analyses, 1. Techniques, *J. geophys. Res.,* **88,** 1222–1228.

Stauning, P. & Primdahl, F., 2000. First detection of global dawn–dusk ionospheric current intensities using Ampere's integral law on Ørsted satellite orbits, *Geophys. Res. Lett.,* **27,** 3273–3276.

Tarantola, A., 1987. *Inverse Problem Theory—Methods for Data Fitting and Model Parameter Estimation,* Elsevier, New York.

Walker, M.R. & Jackson, A., 2000. Robust modelling of the Earth's magnetic field, *Geophys. J. Int.* **143,** 799–808.